PHYSICAL REVIEW B **98**, 161120(R) (2018)

Rapid Communications

Hidden charge order of interacting Dirac fermions on the honeycomb lattice

Elliot Christou,[1] Bruno Uchoa,[2] and Frank Krüger[1,3]

[1]*London Centre for Nanotechnology, University College London, Gordon St., London, WC1H 0AH, United Kingdom*
[2]*Department of Physics and Astronomy, University of Oklahoma, Norman, Oklahoma 73069, USA*
[3]*ISIS Facility, Rutherford Appleton Laboratory, Chilton, Didcot, Oxfordshire OX11 0QX, United Kingdom*

(Received 2 May 2018; published 23 October 2018)

We consider the extended half-filled Hubbard model on the honeycomb lattice for second nearest-neighbor interactions. Using a functional integral approach, we find that collective fluctuations suppress topological states and instead favor charge ordering, in agreement with previous numerical studies. However, we show that the critical point is not of the putative semimetal-Mott insulator variety. Due to the frustrated nature of the interactions, the ground state is described by a novel hidden *metallic* charge order with *semi-Dirac* excitations. We conjecture that this transition is not in the Gross-Neveu universality class.

DOI: 10.1103/PhysRevB.98.161120

I. INTRODUCTION

The extended, half-filled Hubbard model on the honeycomb lattice exhibits a rich phase diagram, even at mean-field level. The low-energy excitations in the semimetallic phase are massless Dirac fermions [1], which couple to the order-parameter fluctuations and are known to change the universal critical behavior to that of the Gross-Neveu-Yukawa (GNY) [2] variety. For the transition from the Dirac semimetal to the antiferromagnetic Mott insulator, driven by the on-site Hubbard repulsion U, this has been well understood through a combination of analytical low-energy theories [3,4] and sign-free auxiliary-field quantum Monte Carlo [5–7].

Of the many broken-symmetry phases driven by nearest-neighbor (NN) and next-nearest-neighbor (NNN) repulsions, topological phases are favored by strong NNN interactions (V_2) [8], which can stabilize the Kane-Mele quantum spin Hall phase (QSH) in the spinful model [9], or the Haldane quantum anomalous Hall (QAH) state in the spinless case [10]. Those states nevertheless compete with unconventional charge order (see Fig. 1) that extends beyond the honeycomb unit cell [11]. One would expect quantum fluctuations to play a crucial role in determining the fate of the topological phases, in particular the soft fluctuations associated with breaking of continuous spin rotational symmetry in the QSH phase. Unfortunately, the sign problem for large V_2 prevents the use of quantum Monte Carlo methods [12]. Extensive numerical research into spinless [13–18] and spinful [19–22] models using exact diagonalization, variational Monte Carlo, infinite density matrix RG, and functional RG have been pivotal to determine the phase behavior.

In this Rapid Communication, we analytically examine the role of fluctuations for the phase competition along the V_2 axis. We derive an effective low-energy description for the quantum phase transition into the charge ordered CDW_3 state and analyze the leading instabilities in the presence of the long-wavelength collective fluctuation fields via a functional integral approach. Our analytical results are convincingly consistent with numerical lattice calculations, which suggest that CDW_3 order is favored over topological Mott insulating phases. However, surprisingly, we find that the onset of CDW_3 order does not produce a many-body Mott gap, but rather a novel hidden metallic order as a result of the frustration of the V_2 interaction on the triangular sublattices. The low-energy excitations of this state are massless *semi-Dirac* quasiparticles [23], which disperse linearly in one direction and parabolically in the other. We show that this state is robust against fluctuation effects. We conjecture that the phase transition to the metallic CDW_3 state is not in the GNY universality class.

II. MODEL AND LOW-ENERGY DESCRIPTION

Our starting model is given by the Hamiltonian

$$\mathcal{H} = -t \sum_{\langle i,j\rangle} \sum_{s=\uparrow,\downarrow} (c^{\dagger}_{is} c_{js} + \text{h.c.}) + V_2 \sum_{\langle\langle i,j\rangle\rangle} \hat{n}_i \hat{n}_j \qquad (1)$$

on the half-filled honeycomb lattice with NN hopping t and NNN repulsion V_2, where c_{is} is an annihilation operator for an electron with spin s on site i and $\hat{n}_i = \hat{n}_{i\uparrow} + \hat{n}_{i\downarrow}$ the density operator. The corresponding spinless model is obtained by suppressing the spin index s. In the absence of interactions, the low-energy theory of the semimetallic state describes massless Dirac fermions at the corners of the Brillouin zone $K_{\nu=\pm} = \frac{4\pi}{3\sqrt{3}}(\nu, 0)$,

$$\mathcal{H}_t = v_F \int_{|\mathbf{p}|\leqslant\Lambda} d\!\!\!^{-2}\mathbf{p}\, \Psi^{\dagger}_{\mathbf{p}} s^0 (p_x \sigma^x \nu^z + p_y \sigma^y \nu^0) \Psi_{\mathbf{p}}, \qquad (2)$$

where v_F is the Fermi velocity, s^{μ}, σ^{μ}, ν^{μ} ($\mu = 0, x, y, z$) are the 4-vectors of identity and Pauli matrices acting, respectively, on the spin, sublattice, and valley spaces and

$$\Psi_{\mathbf{p}} = (\psi^{+\uparrow}_{\mathbf{p}A}, \psi^{-\uparrow}_{\mathbf{p}A}, \psi^{+\uparrow}_{\mathbf{p}B}, \psi^{-\uparrow}_{\mathbf{p}B}, \psi^{+\downarrow}_{\mathbf{p}A}, \psi^{-\downarrow}_{\mathbf{p}A}, \psi^{+\downarrow}_{\mathbf{p}B}, \psi^{-\downarrow}_{\mathbf{p}B}) \qquad (3)$$

is an eight component spinor. The measure $d\!\!\!^{-2}\mathbf{p} = d^2\mathbf{p}N/A$, with $A = 2\pi\Lambda^2$, conserves the number of states N between the lattice and effective models, where Λ is the ultraviolet cutoff.

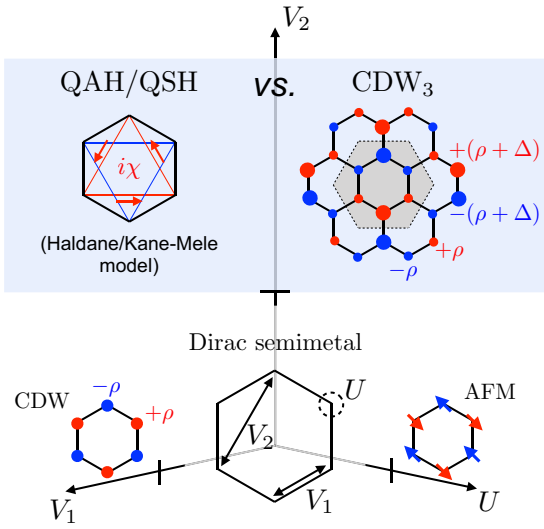

FIG. 1. Schematic phase diagram of the half-filled Hubbard model on the honeycomb lattice. The on-site and NN repulsions U and V_1 induce antiferromagnetic (AFM) and charge-density wave (CDW) states, respectively. At large NNN interactions V_2, there is phase competition between a topological Mott insulator and charge-ordered states with enlarged unit cell (CDW$_3$). The charge modulation is shown relative to half filling.

Decomposition of Hamiltonian (1) in the bond-order order channel, $\hat{\chi}^{\mu}_{ij} = c^{\dagger}_i s^{\mu} c_j$, gives the effective description of the topological Mott insulator states [8]. Enacting the mean-field decoupling in this channel and imposing a translationally invariant, sublattice dependent, and purely imaginary ansatz $\langle \hat{\chi}^{\mu}_{ij} \rangle = i\chi^{\mu}\sigma^z$, which is known to minimize the free energy [8], the effective mass terms are

$$\mathcal{H}_{\chi} = 3V_2 \left(\chi^{\mu}\chi^{\mu} + \frac{\sqrt{3}}{2} \int d^2\mathbf{p}\, \Psi^{\dagger}_{\mathbf{p}} \chi^{\mu} s^{\mu} \sigma^z \nu^z \Psi_{\mathbf{p}} \right), \quad (4)$$

where summation of repeated μ indices is implied. The singlet ($\mu = 0$) component of χ^{μ} describes the order parameter of the QAH phase, which spontaneously breaks global time-reversal symmetry, opening a Mott gap at the Dirac points. Similarly, a nonzero triplet component ($\mu \neq 0$) describes the QSH state, which spontaneously breaks SU(2) spin-rotational symmetry but preserves time-reversal symmetry. The electron mean-field dispersion takes the same form in the QAH and QSH phases, $|\varepsilon_{s\nu}(\mathbf{p})| = \sqrt{v_F^2|\mathbf{p}|^2 + (3\sqrt{3}V_2\chi^{\mu}/2)^2}$.

To describe the competing CDW$_3$ phase (Fig. 1), we decouple the interaction in the density channel and apply the plaquette ansatz [11] for the charge occupation $\langle \hat{n}_i \rangle = \rho_0 + \rho_i$ which describes the deviation of charge occupation $\{\rho_i\} = \{\rho, -\rho, -(\rho+\Delta), -\rho, \rho, \rho+\Delta\}$ from the half filling value $\rho_0 = N_s/2$ (where $N_s = 1$ or 2 is the number of fermionic spin flavors). In total, there are nine equivalent configurations of the CDW$_3$ state related by $2\pi/3$ rotations and translations [13]. The constraints $0 \leqslant \Delta \leqslant \rho \leqslant \rho_0$ and $\rho + \Delta \leqslant \rho_0$ ensure the filling is devoid of pathology. Such a phase spontaneously breaks translational symmetry and keeps only one mirror: $C_{6v} \to C_{1v}$.

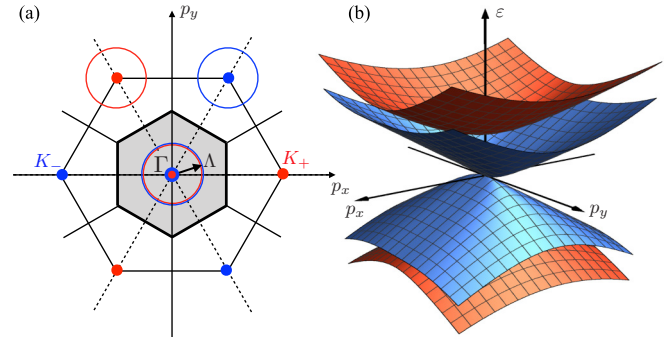

FIG. 2. (a) Gray area: folded Brillouin zone in the CDW$_3$ state. Valleys in the normal state (red and blue dots) fold into the center of the zone. (b) Low-energy bands of the CDW$_3$ state around the Γ point. At half-filling, the system is gapless, with semi-Dirac quasiparticles.

The CDW$_3$ phase is characterized by an enlarged six-site unit cell covering an entire honeycomb plaquette (Fig. 1). The resultant down-folding of the bands increases the number of energy levels at a given momentum threefold. That gives rise to six bands with an additional twofold degeneracy in the spinful model, and maps the Dirac points onto the Γ point ($\mathbf{p} = \mathbf{0}$), as shown in Fig. 2(a). Integrating out the high-energy bands (see Ref. [24]), the interaction part of the Hamiltonian $\tilde{\mathcal{H}} = \tilde{\mathcal{H}}_t + \tilde{\mathcal{H}}_{\delta}$ in the projected space reads

$$\tilde{\mathcal{H}}_{\delta} = \int \tilde{\Psi}^{\dagger}_{\mathbf{p}} s^0 \Big\{ \delta_1 \tau^z \tau^0 + \frac{\delta_2}{2} [C_n \tau^0 (S_m \tau^x - C_m \tau^y) - S_n \tau^z (C_m \tau^x + S_m \tau^y)] \Big\} \tilde{\Psi}_{\mathbf{p}} + E_0, \quad (5)$$

with $\delta_1 = 2V_2(\rho - \Delta)$, $\delta_2 = 2V_2(\rho + \Delta/2)$, $E_0 = (4\delta_2^2 - \delta_1^2)/6V_2$. Here, $C_n = \cos(2\pi n/3)$, $S_n = \sin(2\pi n/3)$ and $n, m = 1, 2, 3$ enumerate the nine possible broken-symmetry state configurations. Written as a combination of irreducible representations [25,26], order parameter δ_1 couples to the charge imbalance between the A and B sublattices, whereas δ_2 couples to the broken rotations (n) and translations (m) of each configuration. The energy dispersion is degenerate up to a $2\pi/3$ rotation, and hence all configurations have the same free energy. In the following, we refer to the $(n, m) = (3, 1)$ pattern in Fig. 1.

In the projected space, $\tilde{\mathcal{H}}_t$ has the same form as in (2) adopting the substitution $\vec{\sigma} \otimes \vec{\nu} \to \vec{\tau} \otimes \vec{\tau}$ to represent the effective, four-dimensional low-energy theory after down-folding and projection. The resulting mean-field dispersion is given by

$$|\tilde{\varepsilon}_{s,\pm}(\mathbf{p})| = \sqrt{v_F^2|\mathbf{p}|^2 + \delta_1^2 + \delta_2^2 \pm 2\delta_2\sqrt{v_F^2 p_y^2 + \delta_1^2}}. \quad (6)$$

III. MEAN-FIELD PHASE DIAGRAM

We expand the Ginzburg-Landau free energy density in terms of the different order parameters. Since there is no evidence for phase coexistence we analyze the cases of QAH/QSH order and CDW$_3$ order separately. This is sufficient to identify the leading instability along the V_2 axis.

For the topological Mott insulators, we obtain the free-energy expansion

$$f_{\rm mf}(\chi) = \alpha_{\rm mf}\chi^2 + \beta_{\rm mf}|\chi|^3 \tag{7}$$

with $\chi = \chi^0$ and $\chi = \chi^z$ in the QAH and QSH phases, respectively. The mean-field coefficients do not depend on the channel in which the symmetry is broken, indicating that at this level, the QAH and QSH phases are degenerate. Note that the presence of a stabilizing cubic term in the free energy is generic for Dirac fermions [27]. For the quadratic coefficient, we obtain $\alpha_{\rm mf} = 3V_2(1-9v_2)$ with $v_2 = \pi\Lambda V_2/v_F A$, indicating a continuous phase transition between the semimetal and a topological Mott insulator at a critical coupling $(v_2)_c = 1/9$.

The analysis is more involved for the CDW_3 state due to the two-gap structure δ_1 and δ_2. Using the parametrization $\Delta = x\rho$ for $0 \leqslant x \leqslant 1$, we obtain

$$f_{\rm mf}(x,\rho) = \tilde{\alpha}_{\rm mf}(x)\rho^2 + \tilde{\beta}_{\rm mf}(x)|\rho|^3, \tag{8}$$

where $\tilde{\alpha}_{\rm mf}(x) = 2V_2[1+2x-6N_s v_2(1-x+\frac{3}{4}x^2)]$ and $\tilde{\beta}_{\rm mf}(x) = 8\pi N_s v_2^2 V_2(2-3x+x^3)$, with $N_s = 1,2$ the spin degeneracy [28]. By inspection, the CDW_3 state with $x=0$ ($\Delta=0$) is the leading instability at a critical coupling $(\tilde{v}_2)_c = 1/(6N_s)$. In the ordered phase, the $\Delta=0$ state remains energetically favorable until large values of V_2 outside the range of applicability of the model.

To summarize, for the spinless case ($N_s=1$), the topological QAH Mott insulator is the leading instability at a critical coupling $(v_2)_c = 1/9$. On the other hand, in the spinful model ($N_s=2$), the transition into the CDW_3 phase occurs at a critical value $(\tilde{v}_2)_c = 1/12$, pre-empting the transition into the QSH phase. These findings are in qualitative agreement with previous mean-field studies on the lattice [11,21,22].

IV. SEMIMETALLIC CHARGE ORDER

In the absence of NN repulsion, the favored charge-ordered state with $\rho > 0$ and $\Delta = 0$ describes a hidden smectic order with gapless excitations. This broken-symmetry state remains *semimetallic*, with one pair of bands opening a gap and another pair remaining gapless, as shown in Fig. 2(b). The effective Hamiltonian matrix of the two gapless bands in the CDW_3 phase is

$$\hat{\mathcal{H}}(\mathbf{p}) = v_F p_x \tau^x + v_F^2 p_y^2/(4V_2\rho)\tau^z, \tag{9}$$

with energy spectrum $|\varepsilon_\pm(\mathbf{p})| = v_F\sqrt{p_x^2 + v_F^2 p_y^4/(4V_2\rho)^2}$. The quasiparticles are *semi-Dirac* fermions, which disperse linearly along the x direction and have a parabolic touching along the y axis. Those touching points sit at the high-symmetry Γ points of the folded Brillouin zone (see Fig. 2).

V. FLUCTUATIONS EFFECTS

Fluctuation corrections to the topological Mott order are best captured by decoupling the interaction in the bond-order channel by means of a Hubbard-Stratonovich transformation. The resultant action $S \sim \int_{\tau,\mathbf{r}} \bar{\psi}(\hat{G}_0^{-1} + iV_2 s^\mu \hat{\chi}^\mu)\psi + V_2\hat{\chi}^\mu\hat{\chi}^\mu$ is quadratic in the fermionic Grassmann fields $\bar{\psi}, \psi$ at the expense of introducing imaginary collective bosonic fields $i\hat{\chi}^\mu_\sigma$. Both vary in position $\mathbf{r}$ and imaginary time τ.

We formulate a self consistent expansion around the broken-symmetry states. This is equivalent to working with the renormalized propagator $\hat{G}^{-1} = \hat{G}_0^{-1} + \hat{\Sigma}$, where $\hat{G}_0^{-1} = \hat{\partial}_\tau - \hat{H}_t$ is the bare fermionic propagator and $\Sigma_s = \frac{3\sqrt{3}}{2}V_2\chi_s\sigma^z\nu^z$ the self-energy due to the zero frequency fields $\chi_s = \chi^0$ or $s\chi^z$ for the QAH and QSH phases, respectively, with $s = \pm$ indexing the spin. Inclusion of the finite frequency fluctuation fields $\tilde{\chi}^\mu_\sigma$ amounts to the addition of a Yukawa coupling to the low-energy effective action, $\mathcal{S} = \mathcal{S}_\psi + \mathcal{S}_{\tilde{\chi}} + \mathcal{S}_{\psi\tilde{\chi}}$, with

$$\mathcal{S}_{\psi\tilde{\chi}} = \frac{3\sqrt{3}}{2}V_2\sum_{\nu\sigma}\int d^3\vec{p}_1 d^3\vec{p}_2\, \bar{\psi}^\nu_{\vec{p}_1\sigma}\tilde{\chi}^\mu_{\vec{p}_1-\vec{p}_2\sigma}s^\mu\psi^\nu_{\vec{p}_2\sigma}. \tag{10}$$

Here, $\vec{p} = (v_F\mathbf{p},\omega)$, $d^3\vec{p} = d^2\mathbf{p}\,d\omega/(2\pi v_F^2)$, and $\nu = \pm$ indexes the valleys.

Integration over the fermionic fields to quadratic order in $\tilde{\chi}$ yields the fluctuation action $\tilde{\mathcal{S}} = \mathcal{S}_{\tilde{\chi}} - \frac{1}{2}\langle\mathcal{S}^2_{\psi\tilde{\chi}}\rangle = \int_{\vec{q}}\tilde{\chi}^\mu_{-\vec{q}\sigma}A^{s'}_{\vec{q}\sigma\sigma'}\tilde{\chi}^\mu_{\vec{q}\sigma'}$, which decouples into the longitudinal $\tilde{\chi}^0$, $\tilde{\chi}^z$ ($s'=s$) and transverse $\tilde{\chi}^x$, $\tilde{\chi}^y$ ($s'=-s$) sectors. The matrix elements

$$A^{s'}_{\sigma\sigma'}(\vec{q}) = \frac{3}{2}V_2\left(\delta_{\sigma\sigma'} + \frac{9}{4}\gamma V_2\sum_s\Pi^{ss'}_{\sigma\sigma'}(\vec{q})\right) \tag{11}$$

depend on the fermionic polarization bubbles $\Pi^{ss'}_{\sigma\sigma'}(\vec{q}) = \sum_\nu\int d^3\vec{p}\,G^{\nu s}_{\sigma\sigma'}(\vec{p}+\vec{q})G^{\nu s'}_{\sigma'\sigma}(\vec{p})$ for the broken symmetry states. In matrix form, $\Pi^{ss'}(\vec{q}) = \Pi^{ss'}_\mu(\vec{q})\sigma^\mu$, where

$$\Pi^{ss'}_0(\vec{q}) \approx \frac{\lambda}{q}\left(q^2+\theta^2+4M^2\frac{q^2-\theta^2}{q^2}+8M_sM_{s'}\right), \tag{12}$$

$$\Pi^{ss'}_x(\vec{q}) \approx -\frac{\lambda}{q}\left(2q^2+v_F^2\mathbf{q}^2+4M^2\frac{v_F^2\mathbf{q}^2-2q^2}{q^2}\right), \tag{13}$$

up to second order in $M_s = 3\sqrt{3}/2V_2\chi_s$, with $\lambda = \pi^2/(8v_F^2A)$, $\vec{q}\cdot\vec{q} = q^2$ and $\Pi^{ss'}_y(\vec{q}) = \Pi^{ss'}_z(\vec{q}) = 0$ [29].

The constant γ in Eq. (11) is a phenomenological parameter that has been included to account for renormalization of the vertex $V_2\tilde{\chi}\bar{\psi}\psi$ from (i) coarse-graining the lattice in a Wilsonian sense; (ii) higher-order $\tilde{\chi}$ terms; and (iii) the Fermi velocity renormalization as $\Pi \propto 1/v_F$. Both the theoretical and experimental evidence for graphene [30–32] suggests $\gamma < 1$. In addition, γ has the added benefit of smoothly interpolating between mean field ($\gamma = 0$) and the bare coupling with fluctuations ($\gamma = 1$).

The Gaussian integrals over the fluctuation fields lead to the free-energy corrections $\delta f_{s'} = \mathrm{Tr}\ln A^{s'}$, from which we obtain the fluctuation contributions to the quadratic coefficients of the Landau expansion,

$$\delta\alpha^\mu_{s'} = \frac{1}{2}\int d^3\vec{q}\ \mathrm{Tr}\left.\frac{\gamma V_2\sum_s\partial^2_{\chi^\mu}\Pi^{ss'}(\vec{q})}{\sigma^0+\gamma V_2\sum_s\Pi^{ss'}(\vec{q})}\right|_{\chi^\mu=0}. \tag{14}$$

Remarkably, it is possible to evaluate the expressions analytically. For the QSH order parameter we obtain

$$\delta\alpha^z_L = \frac{24V_2}{\gamma\pi^2}\left(\mathrm{arccot}^2\Omega - \frac{1}{2}\ln\frac{\Omega^2+3}{\Omega^2+1}\right), \tag{15}$$

$$\delta\alpha^z_T = -\frac{54v_2}{\pi}V_2(1-\Omega\,\mathrm{arccot}\Omega), \tag{16}$$

for the contributions from longitudinal and transverse fluctuations, where $\Omega = \sqrt{8/(9\pi\gamma v_2)-1}$. For the QAH order we

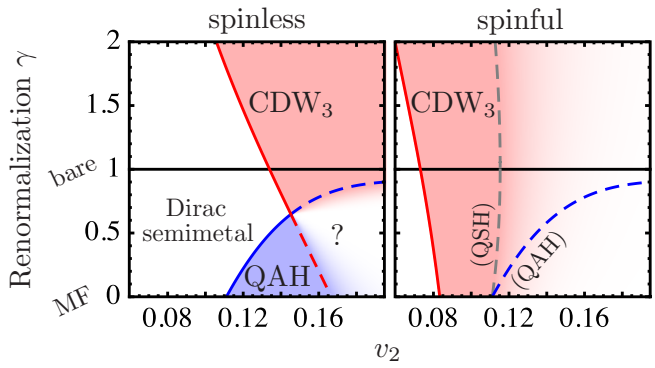

FIG. 3. Lines of critical instability along the $v_2 = \frac{\pi\Lambda}{v_F A} V_2$ axis in the presence of fluctuations, renormalized by the phenomenological parameter γ. The mean-field instabilities are at $\gamma = 0$, the cut $\gamma = 1$ indicates the phase behavior without vertex renormalization. While the critical interaction strengths depend on the momentum cutoff Λ, the order of instabilities does not. In the regime where the NN interactions are zero ($V_1 = 0$), the CDW$_3$ phases are gapless ($\Delta = 0$).

obtain $\delta\alpha_L^0 = \delta\alpha_T^0 = \delta\alpha_L^z$. The calculation breaks down for $v_2 \gtrsim 8/9\pi\gamma$.

In the case of the CDW$_3$ state, the interaction is decomposed in the charge channel by introducing six auxiliary fields $\hat{\rho}_i$ ($i = 1, \ldots, 6$), one for each site in the extended unit cell,

$$\sum_{\langle\langle i,j\rangle\rangle} \hat{n}_i \hat{n}_j = \int_{\vec{q}} \sum_{i,j} \hat{n}_{-\vec{q}i} U_{\mathbf{q}}^{ij} \hat{n}_{\vec{q}j} \to \int_{\vec{q}} \sum_{i,j} \rho_{-\vec{q}i} \left(U_{\mathbf{q}}^{-1}\right)^{ij} \rho_{\vec{q}j} + 2 \int_{\vec{k}\vec{q}} \sum_i \bar{\psi}_{\vec{k}+\vec{q}i} s^0 \psi_{\vec{k}i} \rho_{\vec{q}i}. \quad (17)$$

After projecting into the low-energy fermionic subspace, the calculation proceeds as before. First, we expand around the mean-field solutions, $\rho_i \to \langle\hat{n}_i\rangle + \tilde{\rho}_i$, which dress the fermion propagator. We then integrate over the fermionic fields to obtain the Gaussian action $\tilde{\mathcal{S}} = \int_{\vec{q}} \sum_{ij} \tilde{\rho}_{-\vec{q}i} \tilde{A}_{\vec{q}}^{ij} \tilde{\rho}_{\vec{q}j}$ for the finite-frequency charge fluctuations, where $\tilde{A}_{\vec{q}}^{ij} = (U_{\vec{q}}^{-1})^{ij} + 2\gamma V_2 N_s \tilde{\Pi}_{\vec{q}}^{ij}$, with $\tilde{\Pi}_{\vec{q}}^{ij}$ the charge polarization tensor in the CDW$_3$ phase. Integration over the fluctuation fields gives the leading free energy corrections $\delta\tilde{f} = \mathrm{Tr}\ln\tilde{A}$ in terms of the order parameters ρ and Δ. In general, the coefficients of the expansion can be evaluated numerically. Approximating $U_{\mathbf{q}} \approx U_{\mathbf{q}=\mathbf{0}}$, the quadratic coefficient $\delta\tilde{\alpha}(x)$ ($x = \Delta/\rho$) can be obtained in analytic form [24]. The resulting phase boundaries are almost identical to the ones obtained from numerical integration. We find that fluctuations do not change the nature of the charge order: the CDW$_3$ state remains *metallic* with $\Delta = 0$ ($x = 0$).

VI. PHASE DIAGRAM AND DISCUSSION

Our main results are summarized in Fig. 3. For the spinless model the leading instability at mean field ($\gamma = 0$) is to the topological QAH Mott insulator. Fluctuations favor CDW$_3$ order over the QAH state and are strong enough to cause a continuous phase transition from the Dirac semimetal to the CDW$_3$ phase for $\gamma \gtrsim 0.62$. This is precisely the nature of the transitions found within numerical approaches [14,16–18]. Similar fluctuation-driven changes of the ground state have been recently discussed in terms of a fermionic quantum order-by-disorder mechanism [33–36]. In the spinful model, the transverse fluctuations in the QSH phase stabilize the order, lifting the mean-field degeneracy of the QSH and QAH phases, $\delta\alpha_T^z < 0 < \delta\alpha_L^z = \delta\alpha_{T/L}^0$. The transverse fluctuations are not strong enough, however, to suppress the CDW$_3$ phase, which is the leading instability at mean-field.

The transition to the gapless CDW$_3$ state ($\rho > 0$, $\Delta = 0$) is highly unconventional since the ground state remains metallic with semi-Dirac quasiparticles. It does not belong to the class of putative Dirac semimetal-to-insulator transitions. Instead, the fermion residue remains finite across the transition. This hidden charge order eluded previous numerical studies [13–22] that identified phase transitions through the opening of a Mott gap. The onset of semi-Dirac behavior may be resolved in large-scale DMRG simulations on infinite cylinders, which are now capable of extracting the momentum-dependent excitation spectra of Dirac materials [37]. Finally, with the recent advent of "designer Hamiltonian" methods [7,38] in quantum Monte Carlo it seems possible to engineer the unconventional self-energy terms of the CDW$_3$ state.

By modifying the renormalization-group studies of GNY models [4,39–41], it will be possible to unravel the nature of the quantum critical point and its stability against other couplings. As we demonstrated, the hidden CDW$_3$ order is stable against Gaussian fluctuations. We believe that this stability holds under the RG since the NNN coupling V_2 does not generate interactions between the sublattices that would lift the degeneracy underlying the quadratic touching.

A small NN repulsion V_1 leads to the opening of a Mott gap. Closer inspection shows that the semi-Dirac mode splits into two massive Dirac cones along the quadratic touching direction. While in this case the transition is likely to belong to the chiral Ising GNY universality class, we expect to see a characteristic crossover in the critical fluctuations due the proximity to the unusual critical point at $V_1 = 0$. It has been suggested [22] that the regime of dominant V_2 could become experimentally accessible by using silicon adatoms or cold atoms in double-layers of triangular optical lattices.

In materials with a quadratic band touching, such as bilayer graphene [42], interactions are marginally relevant [43]. Linear terms in the dispersion are generated under the RG, pushing the critical interaction strength back to a finite value and leading to GNY universality [44]. In our case, the bare electron dispersion is already linear. Only because of the matrix structure of the Yukawa coupling for $V_1 = 0$, the symmetry breaking does not lead to the opening of a gap but instead to a quadratic touching along the CDW$_3$ order.

ACKNOWLEDGMENTS

We thank Andrew Green, Andrew James, and Fernando de Juan for useful discussions. B. U. acknowledges NSF CAREER grant No. DMR-1352604 for partial support. F. K. acknowledges financial support from EPSRC under Grant EP/P013449/1.

[1] K. S. Novoselov, A. K. Geim, S. V. Morozov, D. Jiang, M. I. Katsnelson, I. V. Grigorieva, S. V. Dubonos, and A. A. Firsov, Nature (London) **438**, 197 (2005).

[2] D. J. Gross and A. Neveu, Phys. Rev. D **10**, 3235 (1974).

[3] I. F. Herbut, Phys. Rev. Lett. **97**, 146401 (2006).

[4] I. F. Herbut, V. Juričić, and O. Vafek, Phys. Rev. B **80**, 075432 (2009).

[5] F. F. Assaad and I. F. Herbut, Phys. Rev. X **3**, 031010 (2013).

[6] Y. Otsuka, S. Yunoki, and S. Sorella, Phys. Rev. X **6**, 011029 (2016).

[7] T. Sato, M. Hohenadler, and F. F. Assaad, Phys. Rev. Lett. **119**, 197203 (2017).

[8] S. Raghu, X.-L. Qi, C. Honerkamp, and S.-C. Zhang, Phys. Rev. Lett. **100**, 156401 (2008).

[9] C. L. Kane and E. J. Mele, Phys. Rev. Lett. **95**, 226801 (2005).

[10] F. D. M. Haldane, Phys. Rev. Lett. **61**, 2015 (1988).

[11] A. G. Grushin, E. V. Castro, A. Cortijo, F. de Juan, M. A. H. Vozmediano, and B. Valenzuela, Phys. Rev. B **87**, 085136 (2013).

[12] M. Golor and S. Wessel, Phys. Rev. B **92**, 195154 (2015).

[13] N. A. García-Martínez, A. G. Grushin, T. Neupert, B. Valenzuela, and E. V. Castro, Phys. Rev. B **88**, 245123 (2013).

[14] M. Daghofer and M. Hohenadler, Phys. Rev. B **89**, 035103 (2014).

[15] T. Đurić, N. Chancellor, and I. F. Herbut, Phys. Rev. B **89**, 165123 (2014).

[16] S. Capponi and A. M. Läuchli, Phys. Rev. B **92**, 085146 (2015).

[17] J. Motruk, A. G. Grushin, F. de Juan, and F. Pollmann, Phys. Rev. B **92**, 085147 (2015).

[18] D. D. Scherer, M. M. Scherer, and C. Honerkamp, Phys. Rev. B **92**, 155137 (2015).

[19] Y. Volpez, D. D. Scherer, and M. M. Scherer, Phys. Rev. B **94**, 165107 (2016).

[20] D. S. de la Peña, J. Lichtenstein, and C. Honerkamp, Phys. Rev. B **95**, 085143 (2017).

[21] M. Kurita, Y. Yamaji, and M. Imada, Phys. Rev. B **94**, 125131 (2016).

[22] M. Bijelic, R. Kaneko, C. Gros, and R. Valentí, Phys. Rev. B **97**, 125142 (2018).

[23] S. Banerjee, R. R. P. Singh, V. Pardo, and W. E. Pickett, Phys. Rev. Lett. **103**, 016402 (2009).

[24] See Supplemental Material at http://link.aps.org/supplemental/10.1103/PhysRevB.98.161120 for brief descriptions of the calculation of the polarization diagram, derivation of the CDW_3 low-energy theory, and CDW_3 fluctuation calculation.

[25] D. M. Basko, Phys. Rev. B **78**, 125418 (2008).

[26] F. de Juan, Phys. Rev. B **87**, 125419 (2013).

[27] S. Sachdev, *Quantum Phase Transitions*, 2nd ed. (Cambridge University Press, Cambridge, UK, 2011).

[28] The three equivalent CDW_3 orientations allow a "clock term" $(\rho^3 + \rho^{*3}) \sim |\rho|^3 \cos(3\varphi)$ in the free energy. According to the Landau cubic criterion, such cubic terms would render the phase transition first order. Remarkably, the cubic terms scale to zero at the GNY quantum critical point. This is likely to hold for the novel CDW_3 transition, which, like the GNY fixed point, will be characterized by a finite Yukawa coupling and hence fall outside the Landau-Ginzburg-Wilson paradigm. See Ref. [45].

[29] Note that only long-wavelength fluctuations connecting the same Dirac point contribute. Despite interactions, we can assume emergent Lorentz invariance at criticality [4]. Thereby, we can apply the standard field theoretic machinery of Feynman parametrization and dimensional regularization [46,47] to obtain Π (see Ref. [24]).

[30] J. González, F. Guinea, and M. Vozmediano, Nucl. Phys. B **424**, 595 (1994).

[31] D. C. Elias, R. V. Gorbachev, A. S. Mayorov, S. V. Morozov, A. A. Zhukov, P. Blake, L. A. Ponomarenko, I. V. Grigorieva, K. S. Novoselov, F. Guinea, and A. K. Geim, Nat. Phys. **7**, 701 (2011).

[32] V. N. Kotov, B. Uchoa, V. M. Pereira, F. Guinea, and A. H. Castro Neto, Rev. Mod. Phys. **84**, 1067 (2012).

[33] F. Krüger, U. Karahasanovic, and A. G. Green, Phys. Rev. Lett. **108**, 067003 (2012).

[34] F. Krüger, C. J. Pedder, and A. G. Green, Phys. Rev. Lett. **113**, 147001 (2014).

[35] G. Abdul-Jabbar, D. A. Sokolov, C. D. O'Neill, C. Stock, D. Wermeille, F. Demmel, F. Krüger, A. G. Green, F. Levy-Bertrand, B. Grenier, and A. D. Huxley, Nat. Phys. **11**, 321 (2015).

[36] A. G. Green, G. Conduit, and F. Krüger, Annu. Rev. Condens. Matter Phys. **9**, 59 (2018).

[37] Y.-C. He, M. P. Zaletel, M. Oshikawa, and F. Pollmann, Phys. Rev. X **7**, 031020 (2017).

[38] Y.-Y. He, X. Y. Xu, K. Sun, F. F. Assaad, Z. Y. Meng, and Z.-Y. Lu, Phys. Rev. B **97**, 081110 (2018).

[39] J. Zinn-Justin, Nucl. Phys. B **367**, 105 (1991).

[40] L. Rosa, P. Vitale, and C. Wetterich, Phys. Rev. Lett. **86**, 958 (2001).

[41] L. Janssen and I. F. Herbut, Phys. Rev. B **89**, 205403 (2014).

[42] E. McCann and V. I. Fal'ko, Phys. Rev. Lett. **96**, 086805 (2006).

[43] K. Sun, H. Yao, E. Fradkin, and S. A. Kivelson, Phys. Rev. Lett. **103**, 046811 (2009).

[44] S. Pujari, T. C. Lang, G. Murthy, and R. K. Kaul, Phys. Rev. Lett. **117**, 086404 (2016).

[45] Z.-X. Li, Y.-F. Jiang, S.-K. Jian, and H. Yao, Nat. Commun. **8**, 314 (2017).

[46] D. T. Son, Phys. Rev. B **75**, 235423 (2007).

[47] V. N. Kotov, V. M. Pereira, and B. Uchoa, Phys. Rev. B **78**, 075433 (2008).